The multi-scale response of the eddy kinetic energy and transport to strengthened westerlies in an idealized Antarctic Circumpolar Current

Ran Liu[1], Guihua Wang[2], and Dhruv Balwada[3]

[1]Hong Kong University of Science and Technology
[2]Department of Atmospheric and Oceanic Sciences, and Institute of Atmospheric Sciences, Fudan University
[3]Columbia University

March 27, 2024

The multi-scale response of the eddy kinetic energy and transport to strengthened westerlies in an idealized Antarctic Circumpolar Current

Ran Liu[1,2], Guihua Wang[1], and Dhruv Balwada[3]

[1]Department of Atmospheric and Oceanic Science and CMA-FDU Joint Laboratory of Marine Meteorology, Fudan University, Shang Hai, CN
[2]Department of Ocean Science, The Hong Kong University of Science and Technology, Hong Kong, CN
[3]Lamont-Doherty Earth Observatory, Columbia University, Palisades, NY, USA

Key Points:

- Larger eddies got stronger and smaller eddies got weaker as Southern Ocean westerlies strengthened.
- Both flat and ridge channel simulations suggest that these changes may be linked to changes in the inverse energy cascade.
- The corresponding changes in scale-wise meridional and vertical transport are also non-monotonic.

Corresponding author: Guihua Wang, wanggh@fudan.edu.cn

Abstract

The Southern Ocean's eddy response to changing climate remains unclear, with observations suggesting non-monotonic changes in eddy kinetic energy (EKE) across scales. Here simulations reappear that smaller-mesoscale EKE is suppressed while larger-mesoscale EKE increases with strengthened winds. This change was linked to scale-wise changes in the kinetic energy cycle, where a sensitive balance between the dominant mesoscale energy sinks - inverse KE cascade, and source - baroclinic energization. Such balance induced a strong (weak) mesoscale suppression in the flat (ridge) channel. Mechanistically, this mesoscale suppression is attributed to stronger zonal jets weakening smaller mesoscale eddies and promoting larger-scale waves. These EKE multiscale changes lead to multiscale changes in meridional and vertical eddy transport, which can be parameterized using a scale-dependent diffusivity linked to the EKE spectrum. This multiscale eddy response may have significant implications for understanding and modeling the Southern Ocean eddy activity and transport under a changing climate.

Plain Language Summary

The response of eddies in the Southern Ocean to climate change is not well understood. In this study, we used a channel model that simulates the effects of wind on eddies. We found that smaller eddies have less kinetic energy (KE) when the winds are stronger. On the other hand, larger-scale eddies have more KE with stronger winds. Similar phenomena are also observed in the observations. By analyzing the eddy's KE budget, the interaction between different scales of eddies and the interaction between the eddies and mean flow are strengthened when the winds get stronger. This leads to a reduction of eddy KE at smaller mesoscale scales and an increase at larger scales. From the observational view, stronger winds weaken smaller eddies and promote larger waves. This change in eddy KE also affects how eddies meridionally transport materials and how eddy diffusivity varies at different scales. Smaller eddies transport materials less when their KE is weakened, while larger eddies become stronger in transporting materials. These findings determine how eddy diffusivity responds to the changed eddy KE at different scales. The multi-scale response of eddies to wind has important implications for understanding the behavior of Southern Ocean eddies in a changing climate.

1 Introduction

Oceanic eddies play a key role in regulating the Southern Ocean stratification and circulation. These eddies mediate the meridional and vertical exchanges of heat, freshwater, carbon dioxide, nutrients, and other tracers (Ellwood et al., 2020; Frenger et al., 2018; Gnanadesikan et al., 2015; Griffies et al., 2015; Rintoul, 2018; Thompson & Sallée, 2012), while the strong Antarctic Circumpolar Current (ACC) tends to inhibit meridional transport (Siedler et al., 2013). Consequently, the variability of the Southern Ocean eddies has important implications for global ocean circulation and biogeochemical cycles in a changing climate.

The response of eddies to climate change remains an open question and holds particular significance in the Southern Ocean (Rintoul, 2018). Broadly, this inquiry is divided into the response of eddies to two distinct forcings, namely the intensified westerly winds (Swart & Fyfe, 2012; Waugh et al., 2020), and the changing buoyancy forcing in the Southern Ocean (Barkan et al., 2015; Durack et al., 2012; Haumann et al., 2016). Focusing on the strengthened winds, both satellite observations and eddy-resolving models indicated a positive trend in Southern Ocean eddy kinetic energy (EKE) under the historical strengthening of the westerly winds (Morrow et al., 2010; A. M. Hogg et al., 2015; Patara et al., 2016). A similar trend is evident even in global warming simulations (Beech et al., 2022).

The EKE, loosely referred to as eddies, in the ocean is composed of variability over a wide range of scales, which may be referred to as the mesoscales (O($\sim 100-1000$km)), submesoscales (O($\sim\ 1\ -\ 50$km)), finescales (O($\sim\ 100$m)), or described as a series of coherent features, such as Rossby waves, coherent eddies, jets. The mesoscale variability composes the dominant fraction of the EKE in the ocean (Wunsch, 2020), and is associated with the main eddy-driven transport. The observational properties of these mesoscales are usually studied through the satellite-based sea surface height (SSH) (Stammer et al., 2006). Some of these studies focused on identifying and quantifying the properties of mesoscale coherent features in SSH anomaly maps (Chelton et al., 2011), while others quantified the variability over the satellite observable range of spatial-temporal scales ($\sim$ 100km and larger) (Storer et al., 2022; Buzzicotti et al., 2023). To focus on the change in mesoscale EKE under strengthened Southern Ocean winds, Martínez-Moreno et al. (2021) refined the definition of mesoscales as scales smaller than 3^o and found that this mesoscale EKE increased in response to the winds over the past few decades. Alternatively, Busecke and Abernathey (2019) quantified the changes in bulk lateral mixing mainly due to mesoscale eddies and showed that the interannual variability of mixing was linked to climate indices.

While these past studies have shown that EKE and specifically mesoscale EKE have responded to strengthened Southern Ocean winds, the multi-scale response to changing winds remains unknown. The distribution of EKE across spatial-temporal scales is set by many competing mechanisms. The generation of the eddies through baroclinic and barotropic instabilities operate at characteristic scales that respond to large-scale stratification and flow properties (Smith & Marshall, 2009). This variability is then transferred to other scales through non-linear cascades, which may transfer energy to smaller and larger scales (Klein et al., 2019; Balwada et al., 2022; Garabato et al., 2022). The details of these cascades can also be tied to the large-scale flows and forcing, e.g. Liu et al. (2022) showed that the energy in the coherent mesoscale eddy may be transferred to larger scales (Rossby waves) in the presence of stronger zonal flows. Finally, the dissipation mechanisms are also wide and varied, and often linked to boundary processes. In fact, even winds act both as a forcing and a dissipation mechanism, on one hand forcing the large-scale state that leads to instability and then the non-linear cascades, and on the other hand killing eddies by applying a drag on the surface flows (Rai et al., 2021; Torres et al., 2022). Thus, the impact of the changing wind forcing in changing the oceanic EKE, particularly its scale-wise spatial-temporal properties, is non-linear and can be quite complex.

Understanding the multi-scale response of EKE is important for getting a deeper insight into the energetics that shape the ocean circulation, and consequently a better handle on processes setting the ocean storage and transport. While it is understood that the largest eddies do the bulk of the lateral transport in the ocean, processes like the vertical transport of nutrients and ocean ventilation are controlled by flows over a much wider range of scales (Balwada et al., 2018; Uchida et al., 2019). Furthermore, biogeochemical processes interact non-linearly with physical transport over a range of time and space scales (Freilich et al., 2022). Additionally, parameterizations of unresolved sub-grid processes in ocean models are developed by making certain assumptions about energetics (Jansen & Held, 2014; Bachman, 2019), and a better understanding of multi-scale ocean energetics can help inform the improvement and tuning of parameterizations in future ocean models.

To investigate this multi-scale aspect, we performed a scale-wise analysis of changes in the geostrophic EKE in different parts of the ACC (Figure S5). This analysis suggests that the changes in the EKE spectrum at different scales are non-monotonic. For example, observations in the Atlantic sector of the ACC (Figure 1a) indicate an enhancement of larger-scale EKE ($>$ 180km), accompanied by a suppression of smaller mesoscale EKE (90$-$180km). The goal of our study here is to probe the dynamics and corresponding

impact on the transport of such changes. In general, we employ an idealized mesoscale eddy-resolving channel model to investigate the multi-scale response of the EKE in the ACC to strengthened wind forcing. Furthermore, we investigate how these changes impact tracer transport at different scales. Our main finding is that the response of EKE and transport to changing winds is non-monotonic across scales, larger scales get stronger while smaller scales get weaker. We describe our model and analysis methods in section 2, present our main results in section 3, and conclude with a discussion in section 4.

2 Model and Methods

2.1 Model and Experiment Description

This study uses the Massachusetts Institute of Technology general circulation model (MITgcm) (Marshall et al., 1997a, 1997b) to carry out two pairs of channel experiments forced by zonal winds and surface buoyancy restoring. The first pair configuration - channel with flat topography - is similar to Abernathey et al. (2011), which demonstrated the validity of such channel configurations for studying the Southern Ocean. The domain is a square channel of size 2,000km × 2,000km × 4km on a β-plane (β is $1.4E^{-11}$) with a flat bottom. The southernmost Coriolis frequency is $-1.1E^{-4}$. The horizontal resolution is 5km, which is adequate for resolving mesoscale eddies. The vertical grid has 49 levels with spacing increasing from 1 m at the surface to 200m at the bottom. At the surface boundary layer, we use the K-profile boundary layer parametrization (Large et al., 1994). Following Balwada et al. (2018), the numerical viscosity is set by the Modified Leith Viscosity (Fox-Kemper & Menemenlis, 2008). The quadratic bottom drag coefficient is 0.0021. A linear equation of seawater state that depends on temperature is used. Additionally, there is a linear temperature restoration at the surface, with the restoration temperature profile increasing from south to north.

Considering the importance of the bathymetric features in modulating the real ACC flows and EKE (Holloway, 1978; Thompson, 2010; Melet et al., 2013; Howard et al., 2015; Jouanno & Capet, 2020; Zhang et al., 2023), a second pair of experiments were conducted where a topographic ridge was introduced (Abernathey & Cessi, 2014; Balwada et al., 2018). These channel experiments also doubled the domain length, following the setup from Youngs et al. (2023), allowing us to distinguish more clearly between regions closer and away from the ridge. The other physical parameters and initial fields are the same as those in the flat channel.

Both sets of channel simulations were forced by wind stress with a sinusoidal profile, peaking in amplitude in the middle of the domain. The flat bottom experiments have a peak amplitude of $0.1N/m^2$ (FLAT-WIND10) and $0.3N/m^2$ (FLAT-WIND30), and the ridge experiments have peak amplitudes of $0.15N/m^2$ (RIDGE-WIND15) and $0.3N/m^2$ (RIDGE-WIND30). This tripling and doubling of wind is an exaggeration of the actual wind change in the Southern Ocean, which increased by roughly 10% (Lin et al., 2018). However, this large amplification was used following previous studies, e.g. Abernathey et al. (2011); Abernathey and Ferreira (2015b), to clearly see the emerging changes. The change in the wind did not dramatically change the stratification, and the associated deformation radius between the experiments was similar. All experiments were spun up for 50 years before further analysis.

2.2 The Eddy Kinetic Energy Budget

To understand the details of how the mesoscale turbulence changed in response to the winds, we considered the eddy kinetic energy (EKE) budget.

In zonally periodic domains, it is convenient to define the eddy field relative to the zonal mean. The eddy velocity is defined as $u^{'} = u - \overline{u}$ where $\overline{u} = \frac{1}{L_x} \oint u dx$. When

there is no topography, the zonal mean can cleanly separate the zonal mean flow and the time-varying turbulence fields. While in the presence of topography, the variability includes both the time-varying eddies and standing meanders.

The point-wise horizontal EKE ($EKE = 0.5(u'^2 + v'^2)$) budget equation can be constructed by taking the dot product of the horizontal eddy velocity ($U_h^{'} = [u^{'}, v^{'}]$) with the horizontal eddy momentum equation. This results in,

$$\frac{\partial EKE}{\partial t} = -U_h^{'}U^{'} \cdot \nabla U_h^{'} - U_h^{'}\overline{U} \cdot \nabla U_h^{'} - U_h^{'}U^{'} \cdot \nabla \overline{U_h} + U_h^{'}\overline{U^{'} \cdot \nabla U_h^{'}} - \frac{1}{\rho_c}U_h^{'} \cdot \nabla_h P^{'} + U_h^{'} \cdot \mathcal{F}^{'}. \quad (1)$$

Here $U^{'} = [u^{'}, v^{'}, w^{'}]$ is the 3D velocity, $U_h^{'} = [u^{'}, v^{'}]$ is the horizontal velocity, $\nabla = (\partial_x, \partial_y, \partial_z)$ is the 3D gradient operator, $\nabla_H = (\partial_x, \partial_y)$ is the horizontal gradient operator, P' is the pressure perturbation, and $\mathbf{F}^{'}$ is the momentum forcing perturbation.

The first four terms on the right-hand side (RHS) are nonlinear terms relating to how eddies interact with each other and the mean flow. Here the first nonlinear term represents eddy-eddy interactions (named as 'EEE'). The second and third nonlinear terms represent the eddy-mean interactions and are referred to as 'EME' and 'EEM' respectively. The fourth nonlinear term disappears after the zonal average. The fifth term is horizontal pressure work and the last term is the work by the variable forcing. It should be recognized that constant wind forcing does no direct work in the EKE budget, and so can not energize or kill eddies. Further, the horizontal pressure work is rewritten as: $-\frac{1}{\rho_c}U_h^{'} \cdot \nabla_h P^{'} = -\frac{1}{\rho_c}\nabla \cdot (U^{'}P^{'}) + w^{'}b^{'}$. The first term integrates to zero in a domain average. $w^{'}b^{'}$ is usually a source of EKE associated with the baroclinic instability and represents the conversion of the eddy potential energy (EPE) to EKE.

Since this study focuses on the multi-scale nature of the EKE, we considered the scale-wise decomposition of this EKE budget averaged over time and the zonal direction. This scale-wise decomposition was done by analyzing the spectral EKE budget. Since our domain is a re-entrant channel, we only consider the zonal Fourier transform: $\hat{u'}(k) = \int u' e^{ikx} dx$. This obviates the need for any tapering and avoids any associated spectral contamination (Uchida et al., 2019; Schubert et al., 2020). In this spectral space, the horizontal EKE power spectrum is defined as $\widehat{E}(\kappa) = 0.5(\hat{u'}^{\dagger}\hat{u'} + \hat{v'}^{\dagger}\hat{v'})$, where $\hat{(\cdot)}$ and $(\cdot)^{\dagger}$ represent the Fourier transform and its conjugate. Parseval's theorem implies that $\overline{EKE} = \sum_k \widehat{E}(\kappa)$, suggesting that $\widehat{E}(\kappa)$ decomposes the zonal mean EKE into wave components in different spatial scales. The equation for each of these spectral components can be derived in the same way as the equation for the EKE budget, by taking Fourier transforms of the velocity and eddy momentum equation. We used the Python package - xrft (`https://xrft.readthedocs.io/`) for doing all the spectral analysis.

2.3 Tracer Experiments

To study the impact of changing winds on tracer transport, we conducted passive tracer experiments. These tracers were used to estimate the tracer fluxes, eddy diffusivity, and spectral properties of tracer fluxes.

Since the multi-scale response of the spectral EKE to the wind forcing is more clear in the flat channel, we deployed four passive tracers with the following initial concentration profiles in the flat channel experiments:

$$C1 = y; C2 = z; C3 = \cos(\pi y/L_y)\cos(\pi z/H); C4 = \sin(\pi y/L_y)\sin(\pi z/H). \quad (2)$$

These tracers were initialized after the 50-year model spin-up and were evolved for 3 years. Tracer statistics were computed using five-day snapshots from the third month after tracer initialization till the end of the 3 years.

2.4 The spectral decomposition of transport and eddy diffusivity

We investigated the scale-wise characteristics of the transport by assessing the cross-spectra of tracer fluxes (Balwada et al., 2018), which decomposes the meridional and vertical flux of tracers as

$$\overline{v'C'} = \sum_k \hat{v'}\hat{C'}^{\dagger} \tag{3}$$

$$\overline{w'C'} = \sum_k \hat{w'}\hat{C'}^{\dagger}, \tag{4}$$

and provides a sense of how different scales contribute to transport.

Since we compare multiple simulations with different forcing and different EKE levels, the evolution of the passive tracers will be different. So, the tracer flux patterns at any particular time may be impacted by the stage of the tracer evolution. To mitigate this and only compare the properties of transport related to the equilibrated flow and not related to the evolving tracer state we computed the eddy diffusivity. Further, the spectral eddy diffusivity is defined as the ratio of the cross-spectrum of the eddy transport to the background mean gradient of the passive tracer, as suggested by Kong and Jansen (2017). The formula is as follows:

$$D(\kappa) = -\frac{Re(\langle \hat{v'}\hat{C'}^{\dagger} \rangle)}{\partial \langle \overline{C} \rangle / \partial y} \tag{5}$$

Here the eddy transport and its corresponding mean gradient are calculated from the first tracer, $C1$, due to its initial meridional gradient. $\langle \cdot \rangle$ represents the time mean.

Some recent studies estimated the full diffusivity tensor, to relate the eddy tracer flux to its mean gradients (Bachman et al., 2015; Abernathey et al., 2013; Balwada et al., 2019). We also diagnosed this diffusivity tensor, which is why we deployed four tracers in tracer experiments. However, we found that the meridional diffusivity estimated using only the meridional flux and meridional gradient is the same as the major eigenvalue of the diffusivity tensor, which is oriented primarily in the meridional direction. The correlation coefficient of the diffusivity between the two methods is 0.9989 (0.9914) in the FLAT-WIND10 (FLAT-WIND30). Thus, we decided to only present results from the analysis using the simpler estimate of only meridional eddy diffusivity.

We expect the transport properties, quantified in terms of scale-wise diffusivity, to be related to the levels of EKE as a function of scale. One derivation of such a relationship was presented in Kong and Jansen (2017). Based on a barotropic beta plane model, they related the diffusivity to the energy spectrum as follows:

$$D = \int_0^\infty D(\kappa) d\kappa = \frac{1}{C_1} \int_0^\infty \frac{E(\kappa)^{\frac{1}{2}} \kappa^{-\frac{3}{2}}}{1 + \frac{C_2 \beta^2}{2 C_1^2 E(\kappa) \kappa^5}} d\kappa \tag{6}$$

$E(\kappa)$ is the EKE spectrum and κ is the wave number. The two parameters, C_1 and C_2 are empirical parameters, which can be obtained by the least squares fitting. In this study, we estimated these parameters using the FLAT-WIND10 and found that $C_1 = 1.2E^{-3}$ and $C_2 = 9.5E^{-9}$ respectively. We also used this formula and the estimated parameters to predict the scale-dependent diffusivity in the FLAT-WIND30 and found that there was a good agreement - suggesting that the formula works well and the parameters are not very sensitive to the range of flow regimes. We use this formulation to suggest that transport changes are primarily a result of the changes in the energy spectrum.

3 Results

As discussed in the introduction, our observational analysis of the changes in the geostrophic EKE in many sectors of the ACC (sufficiently far away from topography)

found a robust enhancement of larger-scale EKE (> 180km), accompanied by a suppression of smaller mesoscale EKE (90 − 180km) (Figure 1a and Figure S5). This should be viewed in the context of the well-documented acceleration of ACC jets and enhanced total EKE (A. M. Hogg et al., 2015; Shi et al., 2021). To understand the dynamics and implications of the non-monotonic changes in the EKE across scales, we analyze the response of the EKE spectrum in two pairs of experiments.

3.1 The Weakened Smaller-Scale Mesoscale Eddy Kinetic Energy

First, we describe the results from the flat bottom simulations, which are much more qualitatively aligned with the satellite observations. Consistent with previous studies (Abernathey et al., 2011; Abernathey & Ferreira, 2015b), the stronger wind forcing results in a stronger zonal mean flow and EKE (Figure 1b), particularly in the middle of the domain (500-1500km). However, these previous studies have not considered how the EKE changes across different scales. We find that the response of the EKE at different wavenumbers to the strengthened wind is non-monotonic and not the same as the response of the total EKE. The surface EKE spectrum, Figure 1c, shows that the surface EKE increases at scales larger than ∼250km and decreases at scales smaller than ∼250km in the region when the stronger winds drive the stronger zonal jet. The relative change in energy ($\frac{EKE30-EKE10}{EKE10}$) at the large scales is about a factor of 1.29, while the relative change at smaller scales is about a factor of -0.46 (Figure 1c). In addition, the scale below which the EKE is suppressed (above which the EKE is enhanced) remains roughly constant with depth, decreasing very slightly from 267km at the surface to about 227km at 500m (Figure S3).

The scale-wise EKE budgets are useful to investigate the physical processes that result in the scale-wise eddy response to the wind forcing. Here, we consider the terms in the spectral EKE budget corresponding to the conversion of the EPE to EKE ($\overline{w'b'}$), the transfer of kinetic energy due to the eddy-mean interaction (EME and EEM), and the transfer of EKE due to the eddy-eddy interaction (EEE). Figure 1d shows the four terms vertically averaged over the upper 500m, negative values indicate EKE loss, and positive values indicate EKE gain. Generally, the baroclinic instability results in a conversion of EPE to EKE, which results in a peak near ∼250km in these simulations. The largest contributor to the EKE loss near the same scales is the EEE. The EEE also increases the EKE at larger scales, which in combination with the smaller scale energy loss is associated with the inverse energy cascade (Scott & Wang, 2005; Schubert et al., 2020) - transferring the smaller-scale mesoscale EKE to the larger scales. The EEM is smaller than the EEE and does not contribute individually to the inverse energy transfer. The residuals of these four terms are balanced by the pressure work and dissipation.

When the wind forcing is strengthened, there are subtle changes in the aforementioned balance (Figure 1d). Generally, the intensification of EEE and EEM contributes to a greater loss of EKE in the mesoscales and very slight increase at larger scales. Furthermore, the replenishment of mesoscale EKE by the $\overline{w'b'}$ does not show any significant increase in strength. However, it does shift slightly towards larger scales. This shift results in an increased conversion of available eddy potential energy (EPE) to EKE at scales larger than approximately 250 km, while the conversion decreases at scales smaller than the same scales. Additionally, the peaks of EEE and EEM also exhibit a slight shift towards larger scales. It is worth noting that a similar shift towards larger scales in spectral energy budgets has been recently reported for atmospheric flows by (Chemke & Ming, 2020). They found that under changing zonal mean wind and stratification induced by climate change, larger atmospheric waves become stronger while smaller waves become weaker in mid-latitudes.

The experiments with the ridge, Figure 1e, illustrate similar non-monotonic changes of the EKE spectrum in the region 2000km downstream of the ridge. However, the scale where the EKE begins to be suppressed is substantially reduced to a wavenumber of 40km,

and the suppression is much weaker compared to that in the flat channel. The spectral EKE budgets suggest that the weaker mesoscale suppression phenomenon in the ridge case is mainly due to a significant increase in baroclinic eddy energy source $w^{'}b^{'}$ at all scales under intensified westerly (Figure 1f). This increase counteracts the reduction of mesoscale EKE caused by EEE and EEM.

These flat and ridge channels are only idealized analogs for the Southern Ocean, and are not designed to perfectly capture the scales of observed changes, but rather show that wind changes alone can qualitatively describe the observed changes in the EKE at different scales. This initial foray, suggests that the dynamics of actual ACC regions away from topography may lie somewhere between the flat and ridge channels explored here, and more work including more realistic domains and forcing would be needed for quantitative investigation.

3.2 The Suppressed Mesoscale Eddy Transport and Diffusivity

Many previous studies found that eddies play a major role in the meridional transport across the ACC (Volkov et al., 2008; Dufour et al., 2015), and this transport is likely to increase as winds strengthen (A. M. C. Hogg et al., 2008; Spence et al., 2010; Abernathey & Ferreira, 2015b). We expect the same net result in our simulations since the net EKE does increase with increasing winds. In the context of the multiscale response of the spectral EKE to the wind forcing, we consider how the scale-wise eddy transport changes only in the flat channel.

Here we focus on the depth-averaged eddy transport, as there are no significant vertical changes in the EKE and eddy transport (Figure S3). Figure 2 shows the cross-spectrum of the meridional, the vertical eddy transport, and the meridional component of the EKE spectrum. In both experiments, the peak of the meridional eddy transport primarily occurs on scales around 430km within the strong zonal flow (500-1500km), owing to the relatively high EKE levels. Comparing the two experiments, we find that the eddy transport is suppressed in the FLAT-WIND30 for scales smaller than ∼430km but is increased for scales larger than ∼430km. This result can be attributed to the suppression of smaller mesoscale EKE and enhancement of larger-scale EKE. However, the scales at which the eddy transport is suppressed do not perfectly align with the scales where EKE reduction occurs. The cross-over scale for transport is ∼430km, whereas the cross-over scale for the energy spectrum is slightly smaller ∼250km.

Similar to the response of the meridional transport, the vertical transport also shows a non-monotonic response. The qualitative scale-wise vertical transport is different between the two experiments; while most scales are associated with upwelling in FLAT-WIND10, the vertical transport in FLAT-WIND30 changes sign with scale (the net result is still upwelling). Also, the strengthened wind forcing significantly enhances the upwelling transport on scales larger than ∼430km and moderately enhances the downwelling transport on scales ranging from 120 km to 430km. These changes correspond to the different increases in the vertical component of EKE at each scale (not shown). Although the model in this study is only mesoscale resolving and has a weak vertical motion, the different transport directions in different scales may have important implications on biogeochemistry and should be considered in higher-resolution simulations in the future.

The cross-spectrum of eddy transport can be utilized to evaluate the spectral mesoscale eddy diffusivity through equation 4 and further probe the properties of the transport. The pattern of the meridional spectral diffusivity depends mainly on the cross-spectrum of eddy transport (Figure 2). Consequently, the peak of spectral diffusivity also occurs mostly on scales ∼430km. In addition, the mesoscale diffusivity is also suppressed at scales of less than ∼430km. This feature serves as a valuable indicator for evaluating scale-dependent diffusivity theories. Figure 2m and 2n show the spectral diffusivity predicted by the diffusivity spectrum theory proposed by (Kong & Jansen, 2017). The correlation coefficient

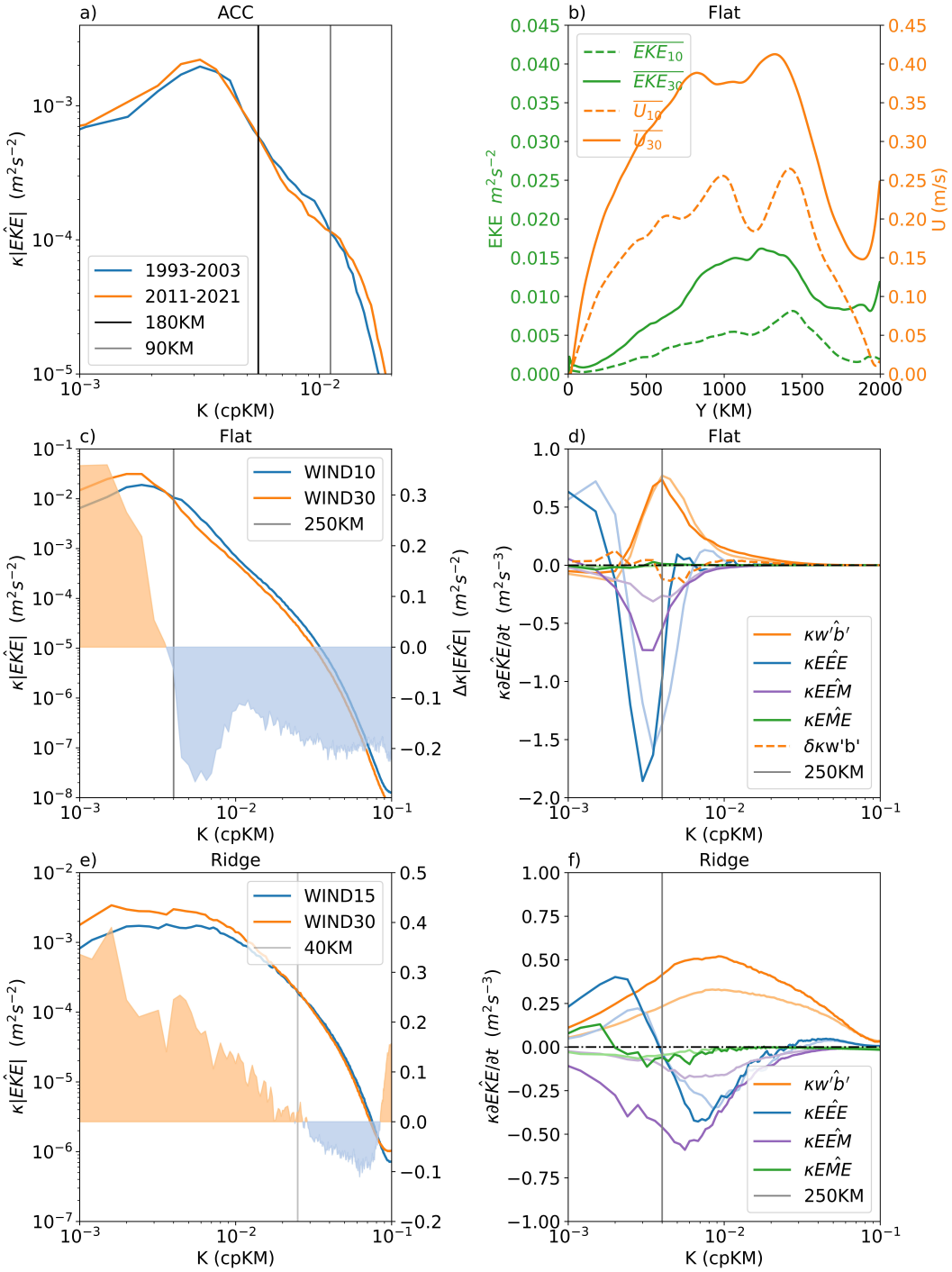

Figure 1. a), The ten-year averaged variance-preserving geostrophic EKE zonal spectrum in the jet region (50°S-45°S) of the ACC Atlantic Section (320°E-360°E) as seen in Figure S5a. The unit is m^2/s^2. b), The zonal and vertical mean zonal velocity and the EKE in the two experiments, where the solid (dashed) lines represent the FLAT-WIND30 (FLAT-WIND10) experiment. The X-axis is the south-north direction in km. The unit of zonal velocity and EKE is m/s and m^2/s^2. c), The meridional averaged variance preserving the EKE spectrum from 500km to 1500km in the two experiments. The unit is m^2/s^2. The orange and blue color shadings indicate the increased and suppressed EKE at each wavenumber, respectively. d), The variance preserving spectral $w'b'$, EEM, EME, and EEE which are meridionally averaged from 500km to 1500km over the upper 500m in the FLAT-WIND10 (light colors) and FLAT-WIND30 (dark colors). The unit is $10^{-9}m^2/s^3$. The orange dashed line shows the difference of the $w'b'$ between the FLAT-WIND30 and the FLAT-WIND10. The unit is m^2/s^3. e), the same as 1c, but for the variance preserving EKE spectrum from 250km to 1100km in the downstream ridge regions, since the latitude positions of the southern branches of the downstream zonal jet are relatively stable, in contrast to the northern branches. f), the same as 1d, but for the two downstream ridge regions.

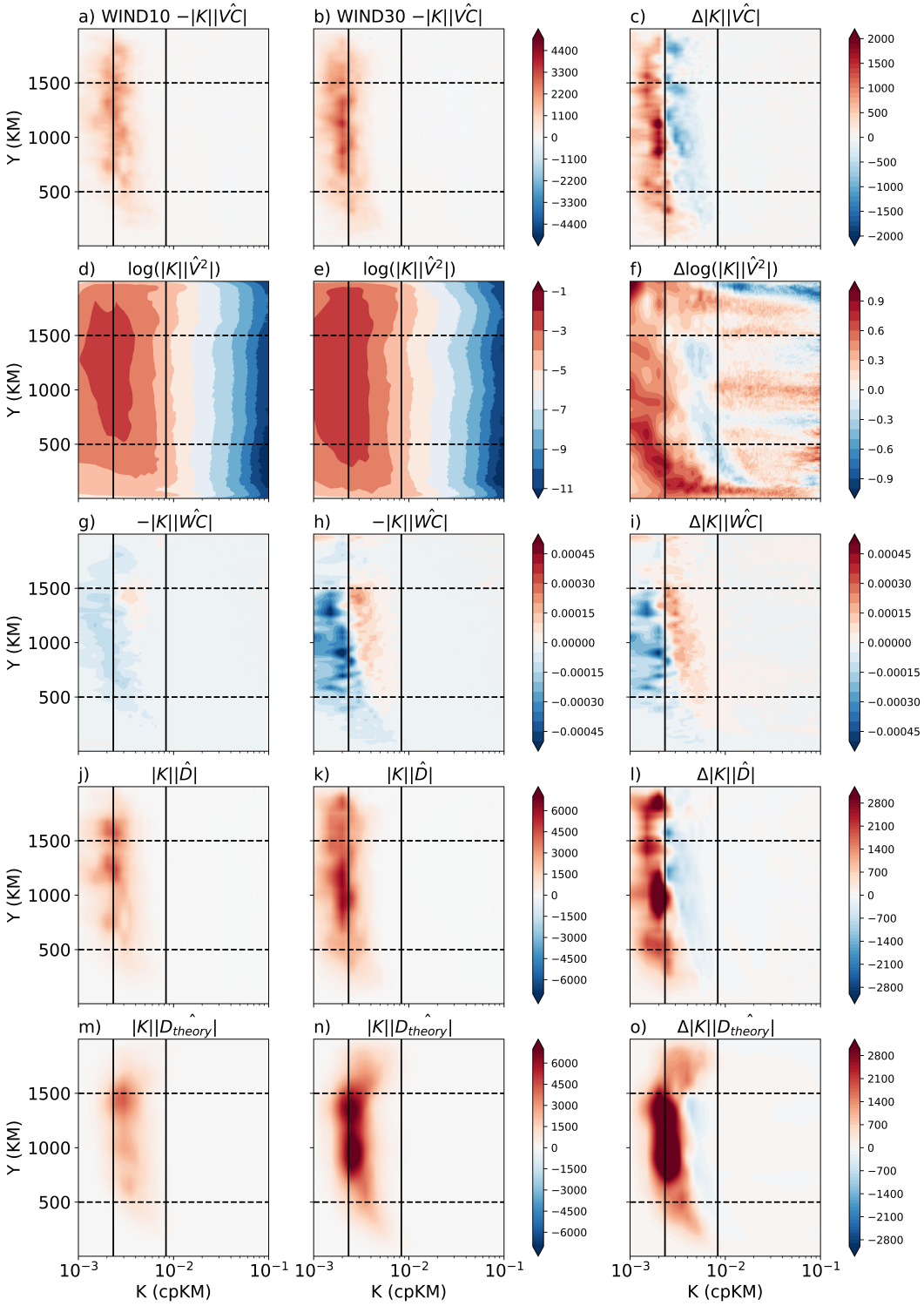

Figure 2. a), The cross-spectrum of the meridional eddy transport in the FLAT-WIND10. The unit is m/s. b), the same as a) but for the FLAT-WIND30. c), the difference in the cross-spectrum of the meridional eddy transport between the two experiments. d), the meridional component of the variance preserving EKE spectrum in the FLAT-WIND10. The unit is $\log_{10} m^2/s^2$. e), the same as 2d but for the FLAT-WIND30. f), the difference in the EKE spectrum between the two experiments. g) The cross-spectrum of the vertical eddy transport in the FLAT-WIND10. The unit is m/s. h), the same as 2g but for the FLAT-WIND30. i), the difference in the cross-spectrum of the vertical eddy transport between the two experiments. j), the diagnosed spectral diffusivity in the FLAT-WIND10. The unit is $\kappa \times m^2 s^{-1}$. k), the same as 2j but for the FLAT-WIND30. l), the difference in the spectral diffusivity between the two experiments. m) theoretical diffusivity in the FLAT-WIND10. The unit is $m^2 s^{-1}$. n), the same as 2m but for the FLAT-WIND30. o), the difference in the theoretical diffusivity between the two experiments. The two solid lines in each figure are the wavelengths at 430km and 120km from left to right The X-axis is the wavenumber, whose unit is km^{-1}. The Y-axis is the cross-frontal

between the integral of the diagnosed and theoretical spectral diffusivity are 0.8890 (FLAT-WIND10) and 0.9356 (FLAT-WIND30) along the meridional direction. In the spectral space, the theory succeeds in predicting the suppressed mesoscale diffusivity as well. This suggests that considering the EKE spectrum, rather than the total EKE, could be beneficial for parameterizing mesoscale diffusivity in the ocean. It should be noted, that the scale of the theoretical suppressed diffusivity peaks at a slightly smaller scale compared with the diagnosed spectral diffusivity. This is because theoretically, the eddy diffusivity is a direct response to the EKE spectrum, thus making the scale of the predicted diffusivity peak dependent on the EKE spectrum peak, while the actual response is slightly different from this theory. This suggests a need to maybe introduce different efficiency of stirring at different scales. However, this investigation is beyond the scope of this work and will be investigated in future theoretical studies.

4 Discussion and Conclusions

The Southern Ocean westerly winds have strengthened over the past few decades. Some recent studies have explored the response of the ocean eddies to the strengthening winds and found that the EKE is increasing. However, none of these studies have tried to investigate whether the EKE is increasing across all scales, or if the EKE at different scales is responding differently to the changing winds. We found the observed multi-scale response of the geostrophic EKE to the changing winds is non-monotonic in regions far away from the topographic ridges. We investigated this multi-scale response of the EKE through idealized channel simulations forced with different wind amplitudes.

Our simulations, similar to past studies, show that the EKE increases as winds strengthen. However, this EKE response is not uniform across spatial scales. In simulations with flat topography, we find that the mesoscale eddies smaller than ~ 250 km are weakened, while the larger eddies are strengthened. In these simulations, this response is the strongest in the top 500m of the domain. It is also worth noting that the scale where the EKE change switches from strengthening to weakening is not fixed, as it can vary depending on different parameters related to the source of eddy energy, including bathymetric features and buoyancy forcings. In the simulations of a ridge, the scales at which the suppression of EKE begins can be significantly reduced to 40 km. Conversely, the scales are expanded to ~ 320 km when the surface buoyancy restoration was turned off (not shown here).

The EKE's non-monotonic response at different scales can likely be linked to non-monotonic changes in the spectral EKE budget. In the flat channel, the stronger zonal jet intensifies eddy-eddy (EEE) and eddy-mean (EEM) interactions, reducing smaller mesoscale EKE and increasing larger-scale EKE, suggesting an intensified inverse kinetic energy cascade. Additionally, the EKE generation also shifts slightly towards larger scales, contributing to the EKE spectrum's non-monotonic response. In the presence of a ridge, although the strengthened EEE and EEM similarly transfer more EKE into larger scales under stronger wind forcing, a significant increase in the baroclinic EKE source counteracts the reduction of smaller-scale mesoscale EKE through the inverse cascade processes. As a result, the phenomenon of mesoscale EKE suppression is weakened. Based on these simulations, it is plausible that the actual ACC falls somewhere between the scenarios of the flat and the ridge channel, since the observed suppression of EKE occurs within the scale range of approximately 180km to 90km.

These non-monotonic changes in the scale-wise statistics may be linked mechanistically to the change in the zonal flow under changing winds. Liu et al. (2022) showed, using both observations and simulations, that stronger jets and zonal flows result in a more rapid loss of eddy energy and shortened eddy lifetime, as this eddy energy is more efficiently converted to larger-scale Rossby waves. In our simulations, the zonal flow speeds up by about 40-50% as the wind strength triples, which could result in a more efficient

conversion of kinetic energy from mesoscale eddies to larger Rossby waves. These processes can be seen by considering the flow structure at different scales. In Figure S4, we show that the simulation with stronger winds has more energetic features at larger scales with meridionally elongated bow-type shapes, which are generally associated with Rossby waves (Early et al., 2011). This enhancement of large-scale wave-like structures comes at the expense of smaller relatively isotropic eddies. This hypothesis is also quantitatively supported by considering the eddy lifetimes, which show that there are significantly fewer mesoscale eddy tracks with longer lifetimes in the FLAT-WIND30 compared to those in the FLAT-WIND10 (Figure S1 and S2).

In summary, the non-monotonic multiscale response of the EKE to the strengthened wind is not trivial but reflects some profound changes in physical processes on different scales. The inverse kinetic energy cascade and the zonal mean flow "killing" smaller-scale mesoscale eddies and facilitating the larger-scale wave activity are the potential mechanisms that lead to the non-monotonic multi-scale responses.

Since the stirring by mesoscale eddies dominates the eddy transport of passive tracers (Klocker & Abernathey, 2014), the non-monotonic multi-scale response of the EKE has important implications for eddy transport and diffusivity. We investigated the detailed properties of eddy transport by considering the cross-spectra of passive tracer flux and the spectral eddy diffusivity. The cross-spectrum of the meridional eddy flux confirmed the suppression (amplification) of turbulent transport at the smaller (larger) scales in the stronger winds. Additionally, we showed that vertical transport also responds non-monotonically to these changes, with the smaller scales starting to oppose the transport by the larger-scale eddies in the stronger wind. This may have non-trivial implications for the biogeochemical tracers, where the time scale of tracer transport and its interactions with different reaction time scales can lead to complex system responses (Freilich et al., 2022).

Further, since the cross-spectrum of the meridional eddy transport is related to the spectral eddy diffusivity, the eddy diffusivity is also enhanced at larger scales but is suppressed at smaller scales. The theoretical formula for scale-dependent diffusivity, derived by Kong and Jansen (2017), generally succeeds in predicting the eddy diffusivity, suggesting that the response of the transport to changing winds is largely linked to changes in the EKE spectrum. This suggests that it is possible to build transport parameterizations for the effects seen in this study by linking the diffusivity to the EKE spectrum, as long as the appropriate EKE spectrum response to changing winds is achieved.

This study is the first to consider the multiscale response of ocean mesoscale eddies to changes in the wind forcing and leaves much room for further investigations into the nature of the eddy response. Future research could utilize more realistic ocean general circulation models to investigate the responses of multi-scale Southern Ocean eddies to surface forcings under climate change in the actual ocean basins. Additionally, while this study focused on mesoscale-resolving processes, it is also important to investigate the role of sub-mesoscale processes in shaping the response of smaller-scale EKE to forcings. Such investigations would contribute to a more comprehensive understanding of ocean eddies' multiscale dynamics and behavior.

5 Open Research

The data used in this study are mainly generated through the model. The model configurations to regenerate the high-frequency output data used in this study and the figures' scripts with the data to produce the figures can be obtained from Ran (2023) . Additionally, the observational geostrophic EKE spectrum data used for analysis in this study were obtained from the delayed-time altimeter gridded products provided by E.U Copernicus Marine Service Information, Marine Data Store (2023). Figures were plot-

ted by using the Python package Matplotlib (The Matplotlib Development Team, 2023). The wavenumber spectra in this study is calculated by using the Python package xrft (Uchida et al., 2023). The mesoscale eddy identification is through the Python package py-eddy-tracker (Delepoulle et al., 2022).

Acknowledgments

RL and GW were supported by the National Natural Science Foundation of China (42030405; 42288101). DB was supported by NSF-OCE-2242110. We truly appreciate the insightful suggestions from two anonymous reviewers and Prof. Andy Hogg that helped enhance the quality of the paper.

References

Abernathey, R., & Cessi, P. (2014). Topographic enhancement of eddy efficiency in baroclinic equilibration. *Journal of physical oceanography*, *44*(8), 2107–2126.

Abernathey, R., & Ferreira, D. (2015b). Southern ocean isopycnal mixing and ventilation changes driven by winds. *Geophysical Research Letters*, *42*(23), 10–357.

Abernathey, R., Ferreira, D., & Klocker, A. (2013). Diagnostics of isopycnal mixing in a circumpolar channel. *Ocean Modelling*, *72*, 1–16.

Abernathey, R., Marshall, J., & Ferreira, D. (2011). The dependence of southern ocean meridional overturning on wind stress. *Journal of Physical Oceanography*, *41*(12), 2261–2278.

Bachman, S. D. (2019). The gm+ e closure: A framework for coupling backscatter with the gent and mcwilliams parameterization. *Ocean Modelling*, *136*, 85–106.

Bachman, S. D., Fox-Kemper, B., & Bryan, F. O. (2015). A tracer-based inversion method for diagnosing eddy-induced diffusivity and advection. *Ocean Modelling*, *86*, 1–14.

Balwada, D., Smith, K. S., & Abernathey, R. (2018). Submesoscale vertical velocities enhance tracer subduction in an idealized antarctic circumpolar current. *Geophysical Research Letters*, *45*(18), 9790–9802.

Balwada, D., Smith, K. S., & Abernathey, R. P. (2019). Measuring eddy driven transport in a zonally inhomogeneous flow. In *22nd conference on atmospheric and oceanic fluid dynamics*.

Balwada, D., Xie, J.-H., Marino, R., & Feraco, F. (2022). Direct observational evidence of an oceanic dual kinetic energy cascade and its seasonality. *Science Advances*, *8*(41), eabq2566.

Barkan, R., Winters, K. B., & Smith, S. G. L. (2015). Energy cascades and loss of balance in a reentrant channel forced by wind stress and buoyancy fluxes. *Journal of Physical Oceanography*, *45*(1), 272–293.

Beech, N., Rackow, T., Semmler, T., Danilov, S., Wang, Q., & Jung, T. (2022). Long-term evolution of ocean eddy activity in a warming world. *Nature climate change*, *12*(10), 910–917.

Busecke, J. J., & Abernathey, R. P. (2019). Ocean mesoscale mixing linked to climate variability. *Science Advances*, *5*(1), eaav5014.

Buzzicotti, M., Storer, B., Khatri, H., Griffies, S., & Aluie, H. (2023). Spatio-temporal coarse-graining decomposition of the global ocean geostrophic kinetic energy. *Journal of Advances in Modeling Earth Systems*, *15*(6), e2023MS003693.

Chelton, D. B., Schlax, M. G., & Samelson, R. M. (2011). Global observations of nonlinear mesoscale eddies. *Progress in oceanography*, *91*(2), 167–216.

Chemke, R., & Ming, Y. (2020). Large atmospheric waves will get stronger, while small waves will get weaker by the end of the 21st century. *Geophysical Research Letters*, *47*(22), e2020GL090441.

Delepoulle, A., evanmason, Clément, CoriPegliasco, Capet, A., Troupin, C., & Koldunov, N. (2022). *Antsimi/py-eddy-tracker (v3.6.1).* [software]. Zenodo. Retrieved from `https://doi.org/10.5281/zenodo.7197432`

Dufour, C. O., Griffies, S. M., de Souza, G. F., Frenger, I., Morrison, A. K., Palter, J. B., ... others (2015). Role of mesoscale eddies in cross-frontal transport of heat and biogeochemical tracers in the southern ocean. *Journal of Physical Oceanography*, *45*(12), 3057–3081.

Durack, P. J., Wijffels, S. E., & Matear, R. J. (2012). Ocean salinities reveal strong global water cycle intensification during 1950 to 2000. *science*, *336*(6080), 455–458.

Early, J. J., Samelson, R., & Chelton, D. B. (2011). The evolution and propagation of quasigeostrophic ocean eddies. *Journal of Physical Oceanography*, *41*(8), 1535–1555.

Ellwood, M. J., Strzepek, R. F., Strutton, P. G., Trull, T. W., Fourquez, M., & Boyd, P. W. (2020). Distinct iron cycling in a southern ocean eddy. *Nature Communications*, *11*(1), 825.

E.U Copernicus Marine Service Information, Marine Data Store. (2023). *Global ocean gridded l 4 sea surface heights and derived variables reprocessed copernicus climate service.* [Dataset]. Retrieved from `https://doi.org/10.48670/moi-00145`

Fox-Kemper, B., & Menemenlis, D. (2008). Can large eddy simulation techniques improve mesoscale rich ocean models? *Washington DC American Geophysical Union Geophysical Monograph Series*, *177*, 319–337.

Freilich, M. A., Flierl, G., & Mahadevan, A. (2022). Diversity of growth rates maximizes phytoplankton productivity in an eddying ocean. *Geophysical Research Letters*, *49*(3), e2021GL096180.

Frenger, I., Münnich, M., & Gruber, N. (2018). Imprint of southern ocean mesoscale eddies on chlorophyll. *Biogeosciences*, *15*(15), 4781–4798.

Garabato, A. C. N., Yu, X., Callies, J., Barkan, R., Polzin, K. L., Frajka-Williams, E. E., ... Griffies, S. M. (2022). Kinetic energy transfers between mesoscale and submesoscale motions in the open ocean's upper layers. *Journal of Physical Oceanography*, *52*(1), 75–97.

Gnanadesikan, A., Pradal, M.-A., & Abernathey, R. (2015). Isopycnal mixing by mesoscale eddies significantly impacts oceanic anthropogenic carbon uptake. *Geophysical Research Letters*, *42*(11), 4249–4255.

Griffies, S. M., Winton, M., Anderson, W. G., Benson, R., Delworth, T. L., Dufour, C. O., ... others (2015). Impacts on ocean heat from transient mesoscale eddies in a hierarchy of climate models. *Journal of Climate*, *28*(3), 952–977.

Haumann, F. A., Gruber, N., Münnich, M., Frenger, I., & Kern, S. (2016). Sea-ice transport driving southern ocean salinity and its recent trends. *Nature*, *537*(7618), 89–92.

Hogg, A. M., Meredith, M. P., Chambers, D. P., Abrahamsen, E. P., Hughes, C. W., & Morrison, A. K. (2015). Recent trends in the s outhern o cean eddy field. *Journal of Geophysical Research: Oceans*, *120*(1), 257–267.

Hogg, A. M. C., Meredith, M. P., Blundell, J. R., & Wilson, C. (2008). Eddy heat flux in the southern ocean: Response to variable wind forcing. *Journal of Climate*, *21*(4), 608–620.

Holloway, G. (1978). A spectral theory of nonlinear barotropic motion above irregular topography. *Journal of Physical Oceanography*, *8*(3), 414–427.

Howard, E., Hogg, A. M., Waterman, S., & Marshall, D. P. (2015). The injection of zonal momentum by buoyancy forcing in a southern ocean model. *Journal of Physical Oceanography*, *45*(1), 259–271.

Jansen, M. F., & Held, I. M. (2014). Parameterizing subgrid-scale eddy effects using energetically consistent backscatter. *Ocean Modelling*, *80*, 36–48.

Jouanno, J., & Capet, X. (2020). Connecting flow–topography interactions, vorticity

balance, baroclinic instability and transport in the southern ocean: the case of an idealized storm track. *Ocean Science*, *16*(5), 1207–1223.

Klein, P., Lapeyre, G., Siegelman, L., Qiu, B., Fu, L.-L., Torres, H., ... Le Gentil, S. (2019). Ocean-scale interactions from space. *Earth and Space Science*, *6*(5), 795–817.

Klocker, A., & Abernathey, R. (2014). Global patterns of mesoscale eddy properties and diffusivities. *Journal of Physical Oceanography*, *44*(3), 1030–1046.

Kong, H., & Jansen, M. F. (2017). The eddy diffusivity in barotropic β-plane turbulence. *Fluids*, *2*(4), 54.

Large, W. G., McWilliams, J. C., & Doney, S. C. (1994). Oceanic vertical mixing: A review and a model with a nonlocal boundary layer parameterization. *Reviews of geophysics*, *32*(4), 363–403.

Lin, X., Zhai, X., Wang, Z., & Munday, D. R. (2018). Mean, variability, and trend of southern ocean wind stress: Role of wind fluctuations. *Journal of Climate*, *31*(9), 3557–3573.

Liu, R., Wang, G., Chapman, C., & Chen, C. (2022). The attenuation effect of jet filament on the eastward mesoscale eddy lifetime in the southern ocean. *Journal of Physical Oceanography*, *52*(5), 805–822.

Marshall, J., Adcroft, A., Hill, C., Perelman, L., & Heisey, C. (1997a). A finite-volume, incompressible navier stokes model for studies of the ocean on parallel computers. *Journal of Geophysical Research: Oceans*, *102*(C3), 5753–5766.

Marshall, J., Hill, C., Perelman, L., & Adcroft, A. (1997b). Hydrostatic, quasi-hydrostatic, and nonhydrostatic ocean modeling. *Journal of Geophysical Research: Oceans*, *102*(C3), 5733–5752.

Martínez-Moreno, J., Hogg, A. M., England, M. H., Constantinou, N. C., Kiss, A. E., & Morrison, A. K. (2021). Global changes in oceanic mesoscale currents over the satellite altimetry record. *Nature Climate Change*, *11*(5), 397–403.

Melet, A., Nikurashin, M., Muller, C., Falahat, S., Nycander, J., Timko, P. G., ... Goff, J. A. (2013). Internal tide generation by abyssal hills using analytical theory. *Journal of Geophysical Research: Oceans*, *118*(11), 6303–6318.

Morrow, R., Ward, M. L., Hogg, A. M., & Pasquet, S. (2010). Eddy response to southern ocean climate modes. *Journal of Geophysical Research: Oceans*, *115*(C10).

Patara, L., Böning, C. W., & Biastoch, A. (2016). Variability and trends in southern ocean eddy activity in 1/12 ocean model simulations. *Geophysical Research Letters*, *43*(9), 4517–4523.

Rai, S., Hecht, M., Maltrud, M., & Aluie, H. (2021). Scale of oceanic eddy killing by wind from global satellite observations. *Science Advances*, *7*(28), eabf4920.

Ran. (2023). *liu-ran/multiscale_response_codes (v1.0.0).* [software]. Zenodo. Retrieved from `https://doi.org/10.5281/zenodo.10260678`

Rintoul, S. R. (2018). The global influence of localized dynamics in the southern ocean. *Nature*, *558*(7709), 209–218.

Schubert, R., Gula, J., Greatbatch, R. J., Baschek, B., & Biastoch, A. (2020). The submesoscale kinetic energy cascade: Mesoscale absorption of submesoscale mixed layer eddies and frontal downscale fluxes. *Journal of Physical Oceanography*, *50*(9), 2573–2589.

Scott, R. B., & Wang, F. (2005). Direct evidence of an oceanic inverse kinetic energy cascade from satellite altimetry. *Journal of Physical Oceanography*, *35*(9), 1650–1666.

Shi, J.-R., Talley, L. D., Xie, S.-P., Peng, Q., & Liu, W. (2021). Ocean warming and accelerating southern ocean zonal flow. *Nature Climate Change*, *11*(12), 1090–1097.

Siedler, G., Griffies, S., Gould, J., & Church, J. (2013). *Ocean circulation and climate: a 21st century perspective.* Academic Press.

Smith, K. S., & Marshall, J. (2009). Evidence for enhanced eddy mixing at mid-depth in the southern ocean. *Journal of Physical Oceanography*, *39*(1), 50–69.

Spence, P., Fyfe, J. C., Montenegro, A., & Weaver, A. J. (2010). Southern ocean response to strengthening winds in an eddy-permitting global climate model. *Journal of Climate*, *23*(19), 5332–5343.

Stammer, D., Wunsch, C., & Ueyoshi, K. (2006). Temporal changes in ocean eddy transports. *Journal of Physical Oceanography*, *36*(3), 543–550.

Storer, B. A., Buzzicotti, M., Khatri, H., Griffies, S. M., & Aluie, H. (2022). Global energy spectrum of the general oceanic circulation. *Nature communications*, *13*(1), 5314.

Swart, N., & Fyfe, J. C. (2012). Observed and simulated changes in the southern hemisphere surface westerly wind-stress. *Geophysical Research Letters*, *39*(16).

The Matplotlib Development Team. (2023). *Matplotlib: Visualization with python (v3.8.2).* [software]. Zenodo. Retrieved from `https://doi.org/10.5281/zenodo.10150955`

Thompson, A. F. (2010). Jet formation and evolution in baroclinic turbulence with simple topography. *Journal of Physical Oceanography*, *40*(2), 257–278.

Thompson, A. F., & Sallée, J.-B. (2012). Jets and topography: Jet transitions and the impact on transport in the antarctic circumpolar current. *Journal of physical Oceanography*, *42*(6), 956–972.

Torres, H. S., Klein, P., Wang, J., Wineteer, A., Qiu, B., Thompson, A. F., ... others (2022). Wind work at the air-sea interface: a modeling study in anticipation of future space missions. *Geoscientific Model Development*, *15*(21), 8041–8058.

Uchida, T., Balwada, D., Abernathey, R., McKinley, G., Smith, S., & Levy, M. (2019). The contribution of submesoscale over mesoscale eddy iron transport in the open southern ocean. *Journal of Advances in Modeling Earth Systems*, *11*(12), 3934–3958.

Uchida, T., Rokem, A., Soler, S., Nicholas, T., Abernathey, R., frederic nouguier, ... Moon, Z. (2023). *xgcm/xrft (v1.0.1).* [software]. Zenodo. Retrieved from `https://doi.org/10.5281/zenodo.7621857`

Volkov, D. L., Lee, T., & Fu, L.-L. (2008). Eddy-induced meridional heat transport in the ocean. *Geophysical Research Letters*, *35*(20).

Waugh, D. W., Banerjee, A., Fyfe, J. C., & Polvani, L. M. (2020). Contrasting recent trends in southern hemisphere westerlies across different ocean basins. *Geophysical Research Letters*, *47*(18), e2020GL088890.

Wunsch, C. (2020). Is the ocean speeding up? ocean surface energy trends. *Journal of Physical Oceanography*, *50*(11), 3205–3217.

Youngs, M. K., Freilich, M. A., & Lovenduski, N. S. (2023). Air-sea co2 fluxes localized by topography in a southern ocean channel. *Geophysical Research Letters*, *50*(18), e2023GL104802.

Zhang, X., Nikurashin, M., Peña-Molino, B., Rintoul, S. R., & Doddridge, E. (2023). A theory of standing meanders of the antarctic circumpolar current and their response to wind. *Journal of Physical Oceanography*, *53*(1), 235–251.